

Fe–Al-rich tridymite–hercynite xenoliths with positive cerium anomalies: preserved lateritic paleosols and implications for Miocene climate

Haibo Zou^{a,b,*}, Kevin D. McKeegan^a, Xisheng Xu^c, Alan Zindler^b

^aDepartment of Earth and Space Sciences, University of California at Los Angeles, Los Angeles, CA 90095, USA

^bNational High Magnetic Field Laboratory and Department of Geological Sciences, Florida State University, Tallahassee, FL 32306, USA

^cDepartment of Earth Sciences, Nanjing University, Nanjing 210093, China

Received 23 September 2003; accepted 19 February 2004

Abstract

We report isotopic and chemical compositions of unusual tridymite–hercynite xenoliths in middle Miocene Niutoushan tholeiites from the southeast coastal area of China. These xenoliths are characterized by positive cerium (Ce) anomalies and extremely high Al₂O₃ (32–34 wt.%) and total iron oxide (20–22%). They have ⁸⁷Sr/⁸⁶Sr of 0.7050–0.7058, ε_{Nd}(0) values of +3.2 to +4.2, ²⁰⁶Pb/²⁰⁴Pb ratios of 18.8–19.1, and δ¹⁸O values of +5.2‰ to +6.1‰. Their chemical and isotopic compositions suggest that these xenoliths represent preserved aluminous lateritic paleosols that are not genetically related to host tholeiites. These lateritic paleosols with strongly desilicated minerals were formed by intense chemical weathering under warm and humid tropical conditions (with annual average temperature of >19 °C and the annual rainfall of >165 cm) in SE China during the interval from 17 to 15 Ma. The formation age of the paleosols corresponds to a period characterized by slow uplift of the Himalayan–Tibetan Plateau region (and thus less consumption of CO₂) after 17 Ma, and eruptions of 17–15 Ma Columbia River flood basalts, the Vogelsberg basalts, and eastern China basalts (and thus more input of CO₂ into the atmosphere). The tridymite–hercynite xenoliths in the Niutoushan basalts thus preserve evidence of extraordinary climatic greenhouse conditions in the middle Miocene that would otherwise have been lost by the erosion of paleosols.

© 2004 Elsevier B.V. All rights reserved.

Keywords: Miocene basalts; Crustal xenoliths; Lateritic paleosols; Miocene paleoclimate; Crustal stable and radiogenic isotopes; Eastern China basalts

1. Introduction

The widely distributed Cenozoic basalts along eastern China, stretching from Wudalianchi in the

northeast to the Hainan Island in the south, are related to continental extension and upwelling of the asthenospheric upper mantle (e.g., Zhou and Armstrong, 1982; Basu et al., 1991; Chung et al., 1994; Zou et al., 2000, 2003), possibly resulting from the India–Eurasia collision (Tapponnier et al., 1986), or back-arc extension due to subduction of the Pacific plate (Tatsumi et al., 1989). There are a variety of xenoliths in these Cenozoic basalts, with spinel peridotites being the most common. An unusual xenolith, con-

* Corresponding author. Department of Earth and Space Sciences, University of California at Los Angeles, Box 951567, Los Angeles, CA 90095-1567, USA. Tel.: +1-310-794-5047; fax: +1-310-825-2779.

E-mail address: hzou@ess.ucla.edu (H. Zou).

sisting of an Fe–Al-rich tridymite–hercynite assemblage, has been observed in the Miocene Niutoushan volcanic cone on the southeast coastal area of China (Zhou, 1981, 1983). Because (1) the occurrence of tridymite–hercynite xenoliths has not been reported anywhere else on the Earth, (2) the nature of these xenoliths is an interesting problem in the fields of petrology and geochemistry, and (3) the origin of these xenoliths is problematic, we carried out detailed isotopic and chemical studies of the xenoliths and their host tholeiites in order to have a better understanding of their origin. We show below that these xenoliths not only bear petrological significance but also have unexpected implications for middle Miocene climates of Southeast Asia.

The Niutoushan volcanic cone is situated in Longhai County, Fujian Province, near the Taiwan Strait, northeast of the South China Sea (Fig. 1). The South China Sea was developed over the time frame 32–16 Ma as a result of Indian–Eurasia collision-induced extensional forces (Tapponnier et al., 1986). A northeastward propagation of stress created a

rifting tectonic region around the Taiwan Strait and resulted in the emplacement of intraplate basalts in the Fujian–Taiwan region, including those basalts in northwestern Taiwan (Chung et al., 1995), Penghu Island (Ho et al., 2000), and Longhai. The Niutoushan basalts from Longhai, covering an area of 0.5 km², erupted at 15.7 ± 0.6 Ma (Ho et al., 2003), and consist mainly of tholeiites, with a small amount of alkali basalts. The alkali basalts contain spinel lherzolite xenoliths and augite megacrysts, whereas the tholeiites contain tridymite–hercynite xenoliths and anorthosite.

The tridymite–hercynite xenoliths, the subject of this study, are observed to the northeast of Niutoushan (Fig. 2). They occur as tabular inclusions (up to $100 \times 15 \times 30$ cm) in the tholeiitic lava flows and are parallel to the flows. The boundaries between xenoliths and host tholeiites are abrupt, with xenoliths being darker (Fig. 3) and denser. The mineral grains are smaller than 50 μ m and have a granular texture. They consist of 50 vol.% hercynite (FeAl₂O₄), 35% tridymite (SiO₂), 2% ilmenite

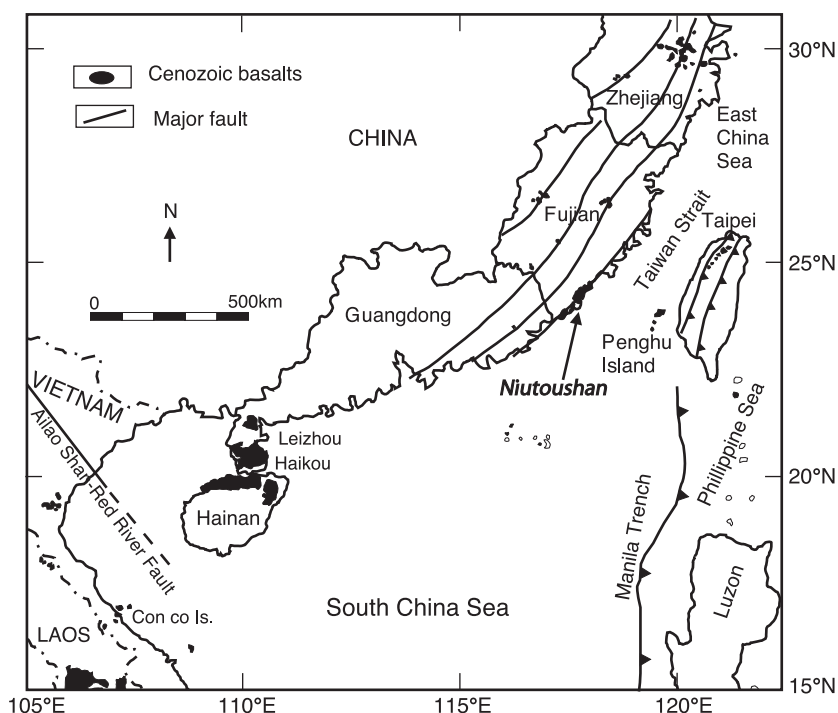


Fig. 1. Location of Niutoushan on the southeast coast of China (revised after Ho et al., 2003).

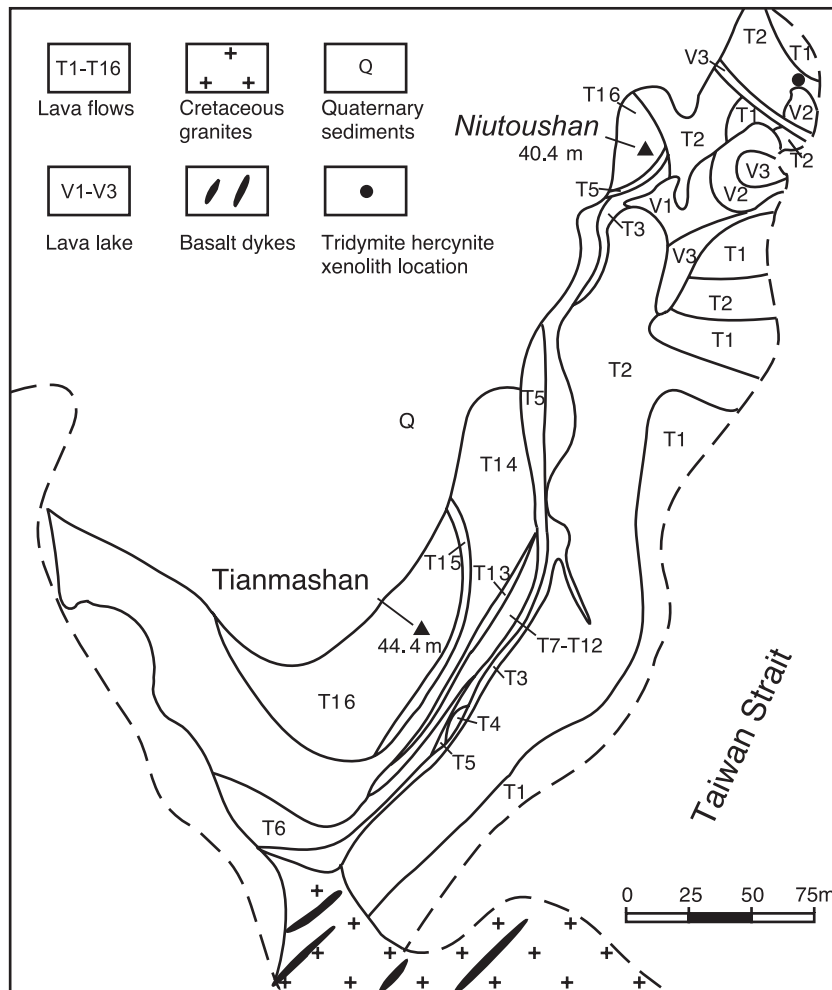


Fig. 2. Location of tridymite–hercynite xenoliths at Niutoushan (revised after Lin, 1992). T1 is the earliest basaltic flow while T16 is the youngest flow. V1 is the oldest lava lake, whereas V3 is the youngest lava lake.

(FeTiO_3), and 10–20% glass (detailed petrographic description and the mineral and glass composition have been documented by Qi et al., 1994). Zhou (1981, 1983) first observed the tridymite–hercynite xenoliths and suggested that they represent the iron-rich residual liquid of highly fractionated tholeiitic magma. Qi et al. (1994) carried out mineralogical and chemical studies of four such xenoliths and disproved formation by extreme tholeiitic fractionation. Although not completely ruling out the possibility of immiscible liquids due to silicate–liquid immiscibility of tholeiitic magma, they prefer that the xenoliths represent the product of a metamor-

phosed sedimentary rock, such as an Fe–Al-rich shale (quartz 5%, kaolinite 75%, and hematite 20%). Because Nd, Sr, Pb and O isotopic compositions are useful tracers in studying petrogenesis, we carried out integrated isotopic and chemical studies of additional xenoliths and their host tholeiites.

2. Analytical methods

Nd, Sr and Pb isotope ratios were measured at the National High Magnetic Field Laboratory (NHMFL) using a Finnigan MAT-262 RPQII mass spectrometer.

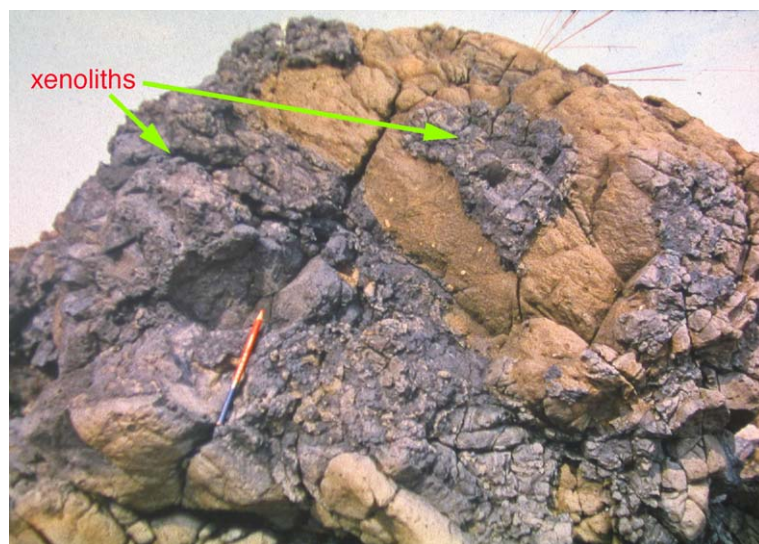


Fig. 3. A field photo of the tridymite–hercynite xenolith in Niutoushan basalts.

Sr and Nd isotopic compositions were normalized to $^{86}\text{Sr}/^{88}\text{Sr}=0.1194$ and $^{146}\text{Nd}/^{144}\text{Nd}=0.7219$, respectively. Measured values for the E&A Sr standard and La Jolla Nd standard were 0.708000 ± 0.000011 (2σ , $n=14$) for $^{87}\text{Sr}/^{86}\text{Sr}$ and 0.511848 ± 0.000011 (2σ , $n=10$) for $^{143}\text{Nd}/^{144}\text{Nd}$, respectively. Replicate analyses of Pb standard NBS-981 gave 36.507 ± 0.012 for $^{208}\text{Pb}/^{204}\text{Pb}$, 15.430 ± 0.004 for $^{207}\text{Pb}/^{204}\text{Pb}$, and 16.891 ± 0.003 for $^{206}\text{Pb}/^{204}\text{Pb}$. Relative to the following values for NBS981: $^{206}\text{Pb}/^{204}\text{Pb}=16.9356$, $^{207}\text{Pb}/^{204}\text{Pb}=15.4891$, and $^{208}\text{Pb}/^{204}\text{Pb}=36.7006$ (Todt et al., 1996), Pb isotopic data in samples were corrected for mass fractionation of 0.13% per atomic mass unit for $^{206}\text{Pb}/^{204}\text{Pb}$, $^{207}\text{Pb}/^{204}\text{Pb}$, and $^{208}\text{Pb}/^{204}\text{Pb}$. Whole-rock O isotope compositions were measured at the Nanjing University on a MAT 252 using the conventional BrF_5 method, which has a reproducibility better than $\pm 0.2\text{‰}$ for $\delta^{18}\text{O}$. Tridymite and quartz oxygen isotopic compositions were measured at UCLA by Cameca IMS 1270 ion microprobe using a 2-nA Cs^+ primary beam focused on a 20 μm diameter spot. Measurements were made by multiple collector Faraday cup detectors at a mass resolving power of 2000. Instrumental mass fractionation was corrected by reference to standard quartz NL 615 ($\delta^{18}\text{O}=18.40\text{‰}$). $\delta^{18}\text{O}$ reproducibility is $\pm 1\text{‰}$. Trace element concentrations were measured at NHMFL using a Finnigan ELEMENT ICP-MS.

Straight sample dissolution procedure was used for ICP-MS measurement. One hundred milligrams of sample powder was dissolved with 3:1 HF/ HNO_3 mixture in 30 ml Savillex beakers. After placing the beakers on the hotplate for 48 h and then evaporating to dryness at 100 °C, samples were re-dissolved in 7N HNO_3 and left in an ultrasonic bath for 45 min. At this stage, most samples were completely dissolved. If incomplete dissolution occurred, samples were heated to 170–200 °C in 7N HNO_3 for several hours and were repeatedly placed in an ultrasonic bath for 10-min intervals, until complete sample dissolution was obtained. Reproducibility for rare earth element concentrations is generally $<2\%$, and reproducibility for other elements is $<5\%$. Detailed analytical methods and results of international rock standards BHVO-1 and BIR-1 have been documented in Stracke et al. (2003). Major element abundances were obtained on fused La-bearing lithium borate glass disks using a Siemens MRS-400 multi-channel, simultaneous X-ray fluorescence (XRF) spectrometer at the Ronald B. Gilmore XRF Lab of the University of Massachusetts at Amherst. Relative errors ($2\sigma/\text{mean}$) for major elements are: SiO_2 (0.4%), TiO_2 (0.4%), Al_2O_3 (0.4%), FeO (0.6%), MnO (1%), MgO (0.5%), CaO (0.2%), Na_2O (0.9%), K_2O (0.4%), and P_2O_5 (2%) (Rhodes, 1996).

Table 1

Major (wt.%) and trace element (ppm) abundances, and Nd, Sr, Pb, and O isotopic compositions of xenoliths and host tholeiites

Samples	Niu-3 xenolith	Niu-4 xenolith	Niu-5 xenolith	Niu-6 xenolith	Niu-7 xenolith	NT-1 TH	NT-2 TH	NT-4 TH	NT-5 TH	NT-9 TH
SiO ₂	43.7	39.5	39.6	44.0	41.02	50.52	49.9	49.6	49.9	50.8
TiO ₂	2.56	2.73	2.97	2.52	2.74	1.36	1.21	0.98	0.97	1.5
Al ₂ O ₃	31.90	34.31	33.86	32.36	34.37	15.81	15.4	16.07	16.62	15.66
Fe ₂ O ₃	20.17	22.33	21.75	19.97	20.15	11.73	11.35	10.95	10.65	11.53
MnO	0.12	0.09	0.08	0.13	0.11	0.18	0.18	0.13	0.12	0.15
MgO	0.38	0.34	0.37	0.3	0.43	7.57	9.51	10.46	9.47	6.94
CaO	0.34	0.21	0.32	0.37	0.38	9.64	9.43	8.98	9.08	9.81
Na ₂ O	0.00	0.00	0.11	0.00	0.42	2.51	2.6	1.91	2.35	2.58
K ₂ O	0.1	0.07	0.11	0.07	0.07	0.31	0.31	0.35	0.4	0.5
P ₂ O ₅	0.16	0.16	0.2	0.14	0.27	0.18	0.17	0.14	0.13	0.19
Total	99.46	99.71	99.33	99.89	99.96	99.8	100.07	99.56	99.64	99.64
SiO ₂ /Al ₂ O ₃	1.35	1.15	1.17	1.36	1.19	3.20	3.24	3.09	3.00	3.24
Mg#	0.03	0.03	0.03	0.03	0.04	0.54	0.60	0.64	0.62	0.52
CIA	0.98	0.99	0.97	0.98	0.96					
1 ⁸ O	0.69	0.68	0.68	0.69	0.68					
Rb	1.38	0.76	3.11	1.38	1.00	4.52	4.41	6.00	7.54	11.6
Ba	443	763	436	386	288	129	141	129	135	155
Th	3.19	3.29	4.24	2.97	3.72	1.43	1.39	1.21	1.21	1.64
U	0.66	0.63	0.76	0.49	0.71	0.28	0.28	0.26	0.25	0.33
Nb	30.8	31.5	36.6	29.4	33.0	15.5	15.0	12.6	13.1	18.2
Sr	58.1	53.5	118.5	62.9	46.3	283	293	313	344	303
Hf	4.65	4.79	5.53	4.42	5.10	2.35	2.25	1.74	1.89	2.66
Zr	195	200	228	183	204	98.0	93.4	73.9	79.7	110
Ti	2.56	2.73	2.97	2.52	2.68	1.36	1.21	0.98	0.97	1.5
Y	13.2	12.7	5.62	14.3	9.09	16.4	15.3	11.4	12.7	18.3
La	9.43	8.86	4.60	8.85	6.23	11.5	11.36	9.24	9.73	13.1
Ce	56.4	48.3	11.8	38.6	21.5	23.4	22.8	18.6	19.5	26.3
Pr	2.95	2.51	1.20	2.69	1.64	3.00	2.86	2.32	2.45	3.37
Nd	12.6	10.7	4.96	11.6	6.98	12.8	12.2	9.84	10.4	14.5
Sm	3.78	2.96	1.36	3.28	1.92	3.25	3.07	2.40	2.59	3.64
Eu	1.30	1.05	0.48	1.14	0.65	1.12	1.05	0.86	0.94	1.25
Gd	3.35	2.78	1.24	3.07	1.88	3.31	3.10	2.38	2.60	3.70
Tb	0.64	0.49	0.22	0.57	0.33	0.53	0.50	0.38	0.42	0.60
Dy	3.90	2.89	1.31	3.47	2.01	3.04	2.84	2.12	2.35	3.36
Ho	0.75	0.55	0.26	0.70	0.39	0.58	0.54	0.41	0.45	0.64
Er	2.14	1.52	0.71	1.96	1.07	1.50	1.42	1.05	1.17	1.66
Yb	2.28	1.44	0.71	1.89	1.05	1.21	1.14	0.84	0.93	1.32
Lu	0.32	0.21	0.10	0.28	0.15	0.17	0.16	0.12	0.13	0.18
Ce/Ce*	2.55	2.43	1.18	1.88	1.58	0.94	0.94	0.94	0.94	0.93
⁸⁷ Sr/ ⁸⁶ Sr	0.705230	0.705865	0.705001	0.705272	0.705113	0.703888	0.703903	0.703921	0.703870	0.703813
2SE	0.000007	0.000007	0.000007	0.000007	0.000008	0.000007	0.000007	0.000008	0.000007	0.000007
¹⁴³ Nd/ ¹⁴⁴ Nd	0.512851	0.512853	0.512803	0.512850	0.512820	0.512830	0.512815	0.512821	0.512827	0.512826
2SE	0.000009	0.000006	0.000010	0.000009	0.000008	0.000007	0.000008	0.000007	0.000008	0.000008
^ε _{Nd}	4.2	4.2	3.2	4.1	3.6	3.7	3.5	3.6	3.7	3.7
²⁰⁸ Pb/ ²⁰⁴ Pb	39.364	39.454	39.379	39.310	39.447	39.220	39.179	39.121	39.031	39.218
²⁰⁷ Pb/ ²⁰⁴ Pb	15.619	15.626	15.638	15.622	15.643	15.626	15.624	15.611	15.629	15.625
²⁰⁶ Pb/ ²⁰⁴ Pb	18.982	19.029	18.981	18.907	19.143	18.941	18.902	18.883	18.768	18.903
δ ¹⁸ O (‰)	5.9	5.6	5.2	5.6	6.1	–	7.3	–	6.6	–

TH = tholeiites.

3. Chemical and isotopic compositions

Major and trace element concentrations and Nd, Sr, Pb, and O isotopic compositions of both xenoliths and

host tholeiites are listed in Table 1. Compared with host tholeiites, the tridymite–hercynite xenoliths have significantly higher Al_2O_3 (>31 wt.%), total iron as Fe_2O_3 (>19%), and TiO_2 (>2.5%), but lower SiO_2 ,

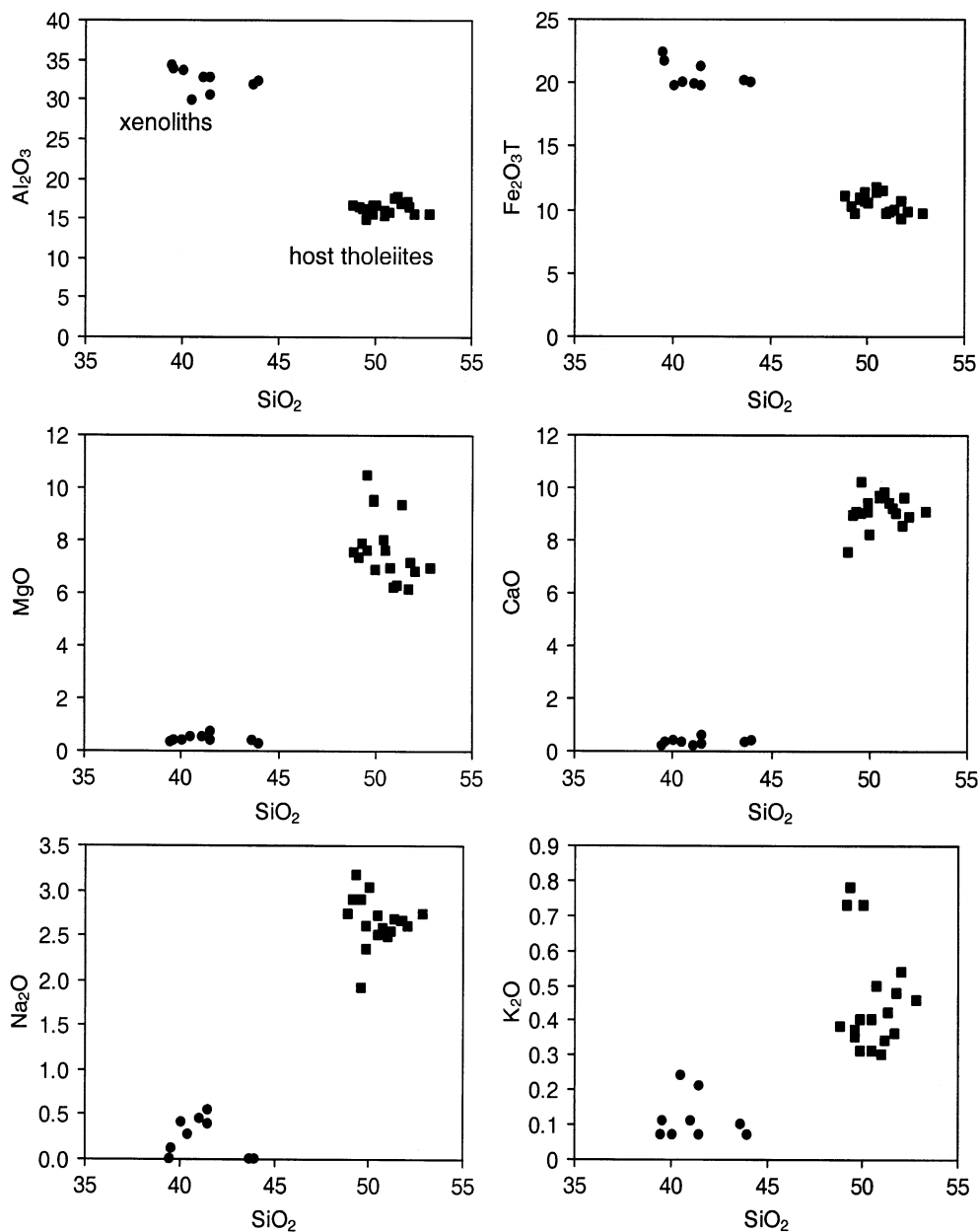


Fig. 4. Plots of wt.% major element oxides vs. SiO_2 for tridymite–hercynite xenoliths and host basalts. Data sources: (Yu, 1985; Qi et al., 1994; this paper).

CaO, MgO, Na₂O, and K₂O (Fig. 4). Both xenoliths and host tholeiites exhibit light-rare-earth-element (LREE)-enriched patterns without significant Eu depletions (Fig. 5). The most striking aspect of the REE abundances of the xenoliths is their significant positive Ce anomalies (with Ce/Ce* = 1.2–2.5). In contrast to host tholeiites, these xenoliths display significant depletions in Rb, and a positive hump in Hf, Zr, and Ti in the primitive-mantle-normalized spider diagram (Hofmann, 1988; Sun and McDonough, 1989) (Fig. 6).

The tridymite–hercynite xenoliths exhibit positive present-day $\epsilon_{\text{Nd}}(0)$ (+3.2 to +4.2), and high $^{87}\text{Sr}/^{86}\text{Sr}$ (0.7050–0.7058) and $^{206}\text{Pb}/^{204}\text{Pb}$ (18.8–19.1). Their $\delta^{18}\text{O}$ values range from +5.2‰ to +6.1‰. When compared with host tholeiites, these xenoliths have significantly higher $^{87}\text{Sr}/^{86}\text{Sr}$, moderately higher $^{206}\text{Pb}/^{204}\text{Pb}$, similar $^{143}\text{Nd}/^{144}\text{Nd}$ (Fig. 7) and lower $\delta^{18}\text{O}$ (Table 1). The tridymite–hercynite xenoliths have higher $^{87}\text{Sr}/^{86}\text{Sr}$ and $^{206}\text{Pb}/^{204}\text{Pb}$ than the mantle peridotite xenoliths (Fig. 7) in the basalts of eastern China (Song and Frey, 1989; Tatsumoto et

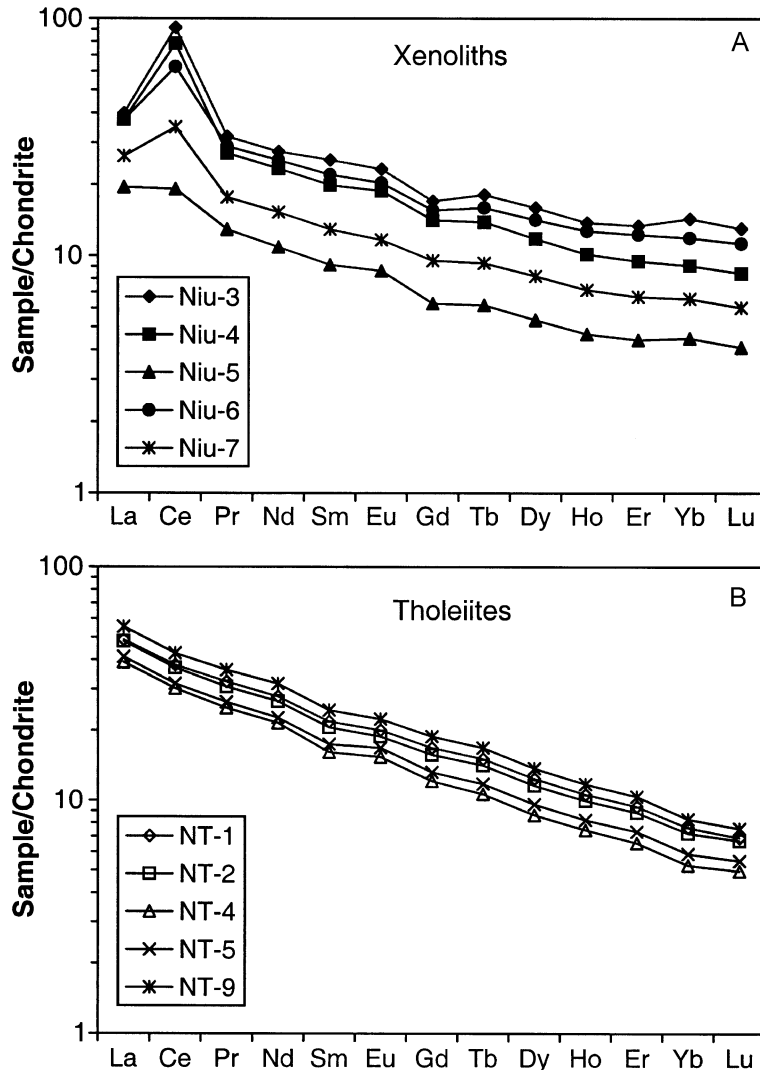


Fig. 5. CI chondrite-normalized rare earth element patterns for xenoliths and host tholeiites. REE abundances for CI chondrites are from Anders and Grevesse (1989).

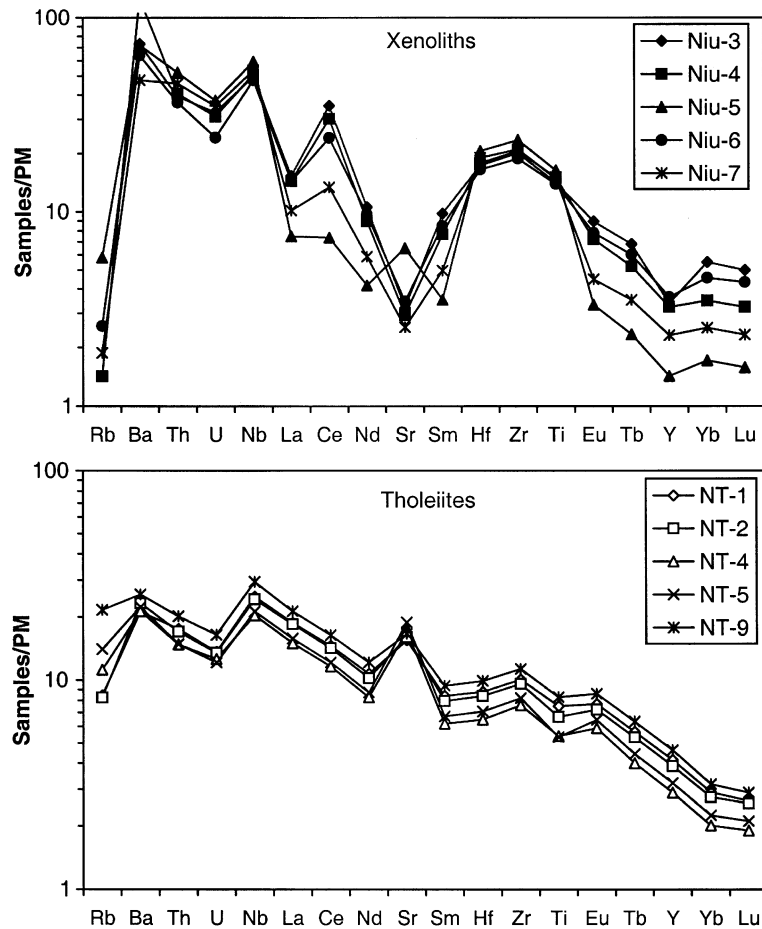


Fig. 6. Primitive-mantle-normalized spider diagrams for xenoliths and host tholeiites. Normalizing values are from Hofmann (1988).

al., 1992; Qi et al., 1995; Fan et al., 2000; Xu et al., 2003).

4. Discussion

4.1. Origin of the tridymite–hercynite xenoliths

The significant differences in $^{87}\text{Sr}/^{86}\text{Sr}$ between tridymite–hercynite xenoliths and their host tholeiites suggest that these xenoliths do not represent an Fe-rich liquid that was derived from tholeiitic magma either by extreme fractionation or by immiscibility. Experiments demonstrate that immiscible iron-rich and silica-poor segregated liquids are relatively alumina-poor ($\text{Al}_2\text{O}_3 < 7.5 \text{ wt.}\%$) (Dixon and Rutherford,

1979), much lower than the xenoliths ($\text{Al}_2\text{O}_3 > 31\%$) studied here. Furthermore, the positive Ce anomalies in these xenoliths indicate oxidation of Ce^{3+} to Ce^{4+} in an oxidizing environment and precipitation as CeO_2 (Banfield and Eggleton, 1989; McLennan, 1989; German and Elderfield, 1990). However, iron-rich residual liquids or immiscible magmas are not related to an oxidizing environment.

The existence of an oxidizing environment inferred from the positive Ce anomalies further argues against the possibility of a mantle or lower crust origin for these xenoliths. Positive Ce anomalies have been observed in the sedimentary rocks at the Earth's surface, mainly in Fe–Mn nodules of the seafloor (Piper, 1974), in fine-grained fractions of pelagic sediments composed almost exclusively of smectites

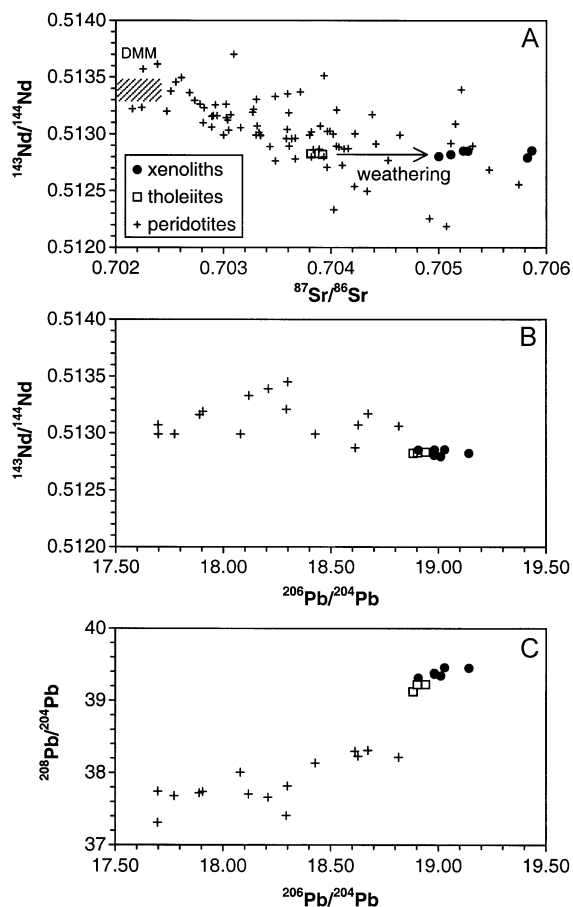


Fig. 7. Nd–Sr, Nd–Pb and Pb–Pb isotopic compositions for tridymite–hercynite xenoliths and host tholeiites. For the cross-hatched box, DMM=depleted MORB source (after Zindler and Hart, 1986). Sr and Nd isotopes for mantle xenoliths are from Song and Frey (1989), Tatsumoto et al. (1992), Qi et al. (1995), Fan et al. (2000) and Xu et al. (2003). Pb isotope data for mantle xenoliths are from Tatsumoto et al. (1992).

(Tlig and Steinberg, 1982), and in the uppermost parts of soil profiles (Morey and Setterholm, 1997; Pan and Stauffer, 2000). The low MnO and high Al₂O₃ in these xenoliths argue against the possibility of Fe–Mn nodules as a protolith. High positive $\epsilon_{\text{Nd}}(0)$ values (+3.2 to +4.2) in the xenoliths also argue against their origin as Fe–Mn nodules or pelagic sediments from Pacific or Indian Ocean because both Fe–Mn nodules and pelagic sediments tend to have negative $\epsilon_{\text{Nd}}(0)$ values (Ben Othman et al., 1989; Abouchami et al., 1997). The very low MgO and K₂O also preclude the presence of smectites (nontronite, saponite, mixed-

layer smectite–illite). Thus, paleosols in the uppermost part of soil profiles appear to be the most likely candidate for the protoliths of the xenoliths. The positive Ce anomalies in the xenoliths support the interpretation of Qi et al. (1994) that the tridymite–hercynite xenoliths are the product of metamorphosed sedimentary rocks. We show below that our integrated isotopic and chemical data provide additional constraints on the nature and formation of these sedimentary rocks.

4.2. The nature of paleosols

The protoliths of the tridymite–hercynite xenolith may not be those of typical paleosols. The very low CaO, Na₂O or K₂O in the xenoliths suggest that there were few if any feldspars, or other potassic clay-mineral alteration products (i.e., illite) in the paleosols. The paleosols could originally have consisted mainly of an aluminous non-potassic low-SiO₂ clay mineral and iron oxyhydroxides (hematite + goethite). The clay mineral is possibly halloysite (ideally Al₂O₃·2SiO₂·4H₂O) because the SiO₂/Al₂O₃ ratio (1.25 ± 0.11) of the xenoliths is similar to the ratio (1.22) of halloysite (Deer et al., 1992). This possibility would suggest that there was little quartz in the original protolith and thus the abundant tridymite in the xenoliths must be mostly of metamorphic origin. Although a few large quartz grains (about 1 mm in diameter) can be observed in the xenoliths, ion microprobe measurements yield $\delta^{18}\text{O}$ of quartz grains (7.2 ± 1.0‰) that are indistinguishable from the isotopic compositions measured for small (<50 μm) tridymite grains (~8.0 ± 0.6‰) in the matrix (Fig. 8). It is known that tridymite is slightly enriched in $\delta^{18}\text{O}$ relative to quartz at isotope equilibrium, but equilibrium oxygen isotope fractionations between tridymite and quartz are small, only 0.2–0.3‰ at 1200–1000 °C (Zheng, 1993), and the polymorphic transformation from tridymite to quartz results in quartz inheriting the oxygen isotopic signature of its precursor tridymite (Zheng, 1995, 1999). Therefore, the similarity in $\delta^{18}\text{O}$ between quartz and tridymite suggests that these large grains were also of metamorphic origin and do not represent the quartz originally in the sediment.

The chemical and isotopic evidence suggests that the paleosols were probably ferruginous bauxites or,

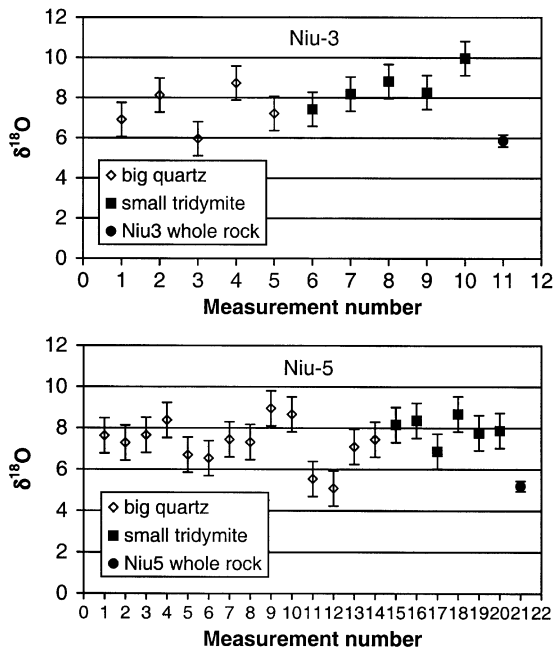


Fig. 8. Quartz and tridymite oxygen isotopic compositions in Niu-3 and Niu-5. The large quartz grains and matrix tridymite in Niu-3 have $\delta^{18}\text{O}$ values of 7.3 ± 1.0 , 8.1 ± 0.6 , respectively. In Niu-5, large quartz grains and matrix tridymite have $\delta^{18}\text{O}$ values of 7.2 ± 1.0 , 7.9 ± 0.6 , respectively. Whole-rock $\delta^{18}\text{O}$ for Niu-3 (5.9 ± 0.2) and Niu-5 (5.2 ± 0.2) are also plotted for comparison.

more likely, aluminous laterites. However, they were not typical laterites, either. Although low, CaO is significantly higher than typical lateritic paleosols, and it would be unusual for laterites to have CaO/K₂O greater than 1. In fact, the xenoliths have high CaO/K₂O ranging from 2.9 to 5.3, whereas a lateritic soil from southeastern China has CaO (0.19%) < K₂O (0.23%) (Xie et al., 1989). A likely explanation is that there was a small carbonate component added to the paleosols. The relatively high content of Ba is also surprising. But Ba can be retained as secondary Basulphate (BaSO₄) that is resistant to acid leaching, with SO₄²⁻ deriving either from groundwater or from original sulphides (Price et al., 1991). Hematite and goethite in the paleosols are mainly of Fe³⁺, whereas hercynite and ilmenite in the xenoliths are dominated by Fe²⁺. The transformation of the hematite–goethite-rich paleosols into the tridymite–hercynite–ilmenite-rich assemblages requires low oxygen fugacity. Experiments suggest that such a transformation may take place at 0.1 kPa (Takahashi et al., 2000).

Organic matter probably also existed in the paleosols, and was responsible for the extraordinary reduction in the oxidation state during the transformation. However, before the paleosols were captured by host basalts, organic matter in the paleosols was not able to reduce CeO₂ to Ce³⁺ at surface conditions, thus retaining the positive Ce anomalies.

Additionally, there are interesting positive correlations among Ce/Ce*, ⁸⁷Sr/⁸⁶Sr and La contents in these xenoliths (Fig. 9). If the amplitude of the Ce anomaly changes with depth, then these xenoliths actually constitute a vertical paleosol sequence. Positive correlations between Ce/Ce* and ⁸⁷Sr/⁸⁶Sr could reflect variable extents of weathering in the soil profile. The observed positive correlation between Ce/Ce* and La is consistent with the report by Pan and Stauffer (2000) that positive Ce anomalies in the uppermost maroon paleosol are accompanied by notably higher LREE contents.

Not all lateritic soils display positive Ce anomalies. For example, in four lateritic profiles from Cameroon, which represent the main lateritic weathering profiles in the tropical zone, positive Ce anomalies have been only found systematically at the top of the saprolite,

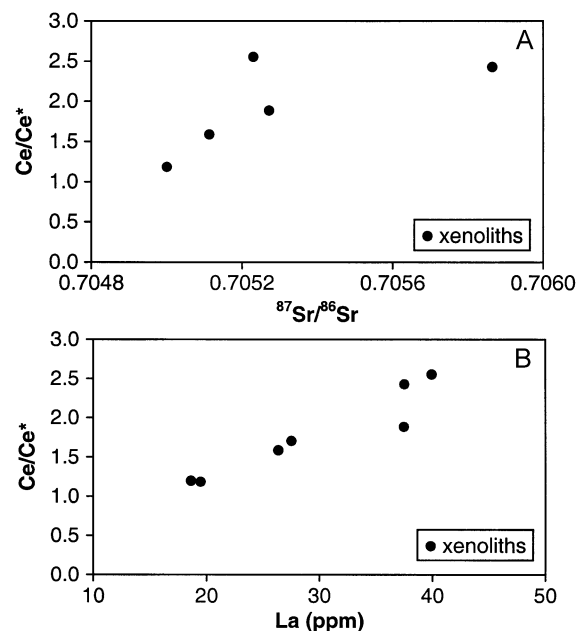


Fig. 9. Ce/Ce* vs. ⁸⁷Sr/⁸⁶Sr (A) and Ce/Ce* vs. La (B) diagrams for xenoliths.

about 4 to 8 m below surface (Braun et al., 1990). The restricted occurrence of Ce anomalies in the uppermost parts of soil profiles makes this feature susceptible to removal by erosion (Pan and Stauffer, 2000), but fortunately, they are apparently preserved in modified form as xenoliths in the Miocene Niutoushan basalts.

4.3. Source rocks for lateritic paleosols

If our interpretation of the xenoliths as metamorphosed paleosols is correct, we can use the Nd isotopic compositions to trace the source rocks for the paleosols because ϵ_{Nd} is not sensitive to interactions with water. Positive $\epsilon_{\text{Nd}}(0)$ (3.2–4.2) in the xenoliths suggests that the source rocks of the paleosols are igneous rocks with a depleted mantle geochemical signature. The dominant rock types from the study region are metasedimentary rocks, Cretaceous granites, and Mesozoic volcanic rocks. The metasedimentary rocks have negative $\epsilon_{\text{Nd}}(0)$ ranging from -3.0 to -4.7 , and Cretaceous granites also have negative $\epsilon_{\text{Nd}}(0)$ ranging from -5.0 to -7.7 (Huang et al., 1986) (Fig. 10). Therefore, it is unlikely for them to be the source rocks for the paleosols. In addition, because granites often exhibit negative Eu anomalies due to fractional crystallization of plagioclase, the absence of Eu anomalies in the xenoliths also argues against granites being source rocks. The Mesozoic volcanic rocks in the Fujian province are rhyolitic tuff, rhyolitic ignimbrite, andesite, and basalt. The intermediate to silicic volcanic

rocks have negative $\epsilon_{\text{Nd}}(0)$, ranging from -5.5 to -11.7 (Huang et al., 1986), and the Mesozoic basaltic rocks also have negative $\epsilon_{\text{Nd}}(0)$ (-2.1 to -10.5) (Xie et al., 2001) (Fig. 10). Thus, these Mesozoic volcanic rocks cannot be source rocks, either.

In contrast to Mesozoic rocks, Cenozoic basalts in the study region mostly have positive $\epsilon_{\text{Nd}}(0)$. The Hainan Island basalts have $\epsilon_{\text{Nd}}(0)$ ranging from 3.6 to 5.7 (Tu et al., 1991), and the Vietnamese basalts have $\epsilon_{\text{Nd}}(0)$ ranging from -0.9 to 7.6 (Nguyen et al., 1996). Since they erupted later than the Niutoushan basalts, these basalts cannot be the source rocks for the xenoliths. Although the Miocene (23–20 Ma) northwestern Taiwan basalts are older than the Niutoushan basalts, their $\epsilon_{\text{Nd}}(0)$ (4.9–5.5) (Chung et al., 1995) is higher than those of the xenoliths [$\epsilon_{\text{Nd}}(0) = 3.2$ –4.2]. We thus regard the nearby Miocene basalts from the earlier (17 Ma) eruptions (Chen and Zhang, 1992; Ho et al., 2003) at Niutoushan, Tianmashan (Fig. 2), Zhenhai, Liuhui, and Xianshan, all in Longhai County, as the most likely source rocks for the paleosols that were metamorphosed to produce the xenoliths.

Surface water and groundwater are enriched in Sr with higher $^{87}\text{Sr}/^{86}\text{Sr}$ (>0.708) than the nearby earlier Miocene basalts, but contain little Pb and even less Nd. Consequently, weathering of such basalts can result in large variations in $^{87}\text{Sr}/^{86}\text{Sr}$, moderate variations in $^{206}\text{Pb}/^{204}\text{Pb}$, and near constant $^{143}\text{Nd}/^{144}\text{Nd}$ in paleosols. The lower whole-rock $\delta^{18}\text{O}$ ($+5.2\text{‰}$ to $+6.1\text{‰}$) of the xenoliths compared to their host basalts ($+6.6\text{‰}$ to $+7.3\text{‰}$) (Table 1) can be attributed to interactions with meteoritic water and groundwater during chemical weathering of the nearby earlier Miocene basalts. Weathering under tropical conditions can leach away K and Rb, but preferentially retain immobile elements Hf, Zr, and Ti, resulting in the depletions in Rb and the hump in Hf, Zr, and Ti. Complete melting of paleosols and subsequent rapid crystallization of the produced liquid would preserve the chemical and isotopic signatures of the paleosols.

The crystallization conditions can be constrained by xenolith mineralogy and oxygen isotope compositions. Based on the phase equilibrium diagram in $\text{FeO}-\text{Al}_2\text{O}_3-\text{SiO}_2$ system obtained by Schairer and Yagi (1952), the crystallization temperature of tridymite–hercynite xenolith is between 1073 and 1205 °C (Qi et al., 1994). This temperature range can be

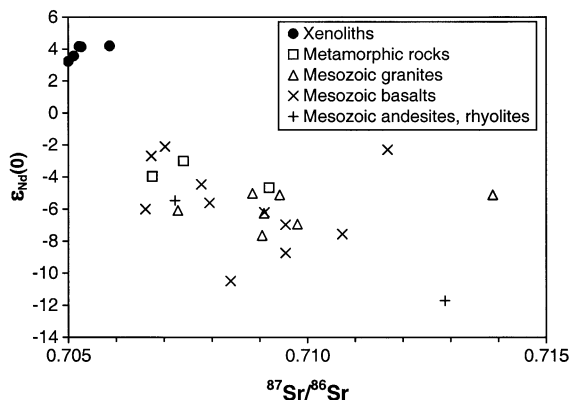


Fig. 10. Comparison of the Nd–Sr isotopic compositions of the xenoliths with those of Mesozoic granites, basalts, andesites, rhyolites and metamorphic rocks.

used to check oxygen isotope equilibrium/disequilibrium. According to Eqs. (4), (5), and (6) in Zhao and Zheng (2003), the oxygen isotope fractionation factor ($10^3 \ln \alpha_{\text{qz-rock}}$) between quartz and whole rock under equilibrium conditions can be expressed as

$$\begin{aligned} \Delta_{\text{rock}}^{\text{qz}} &= 10^3 \ln \alpha_{\text{qz-rock}} \\ &= (1 - I^{18}\text{O}_{\text{rock}}) \times 11.83 \times \frac{10^6}{T^2} \end{aligned} \quad (1)$$

where $I^{18}\text{O}_{\text{rock}}$ is the oxygen isotope index of the whole rock (Zhao and Zheng, 2003), and T is the absolute temperature. The $I^{18}\text{O}_{\text{rock}}$ values of the xenoliths, calculated using Eq. (1) in Zhao and Zheng (2003), as well as oxygen isotopic indices of modal minerals in Zheng (1991) and basalt glass in Zhao and Zheng (2003) are 0.68–0.69 (listed in Table 1). The calculated equilibrium $\Delta^{18}\text{O}$ values between quartz and such xenoliths are 2.1–1.7‰ at 1073–1205 °C, respectively, which is similar to the measured $\Delta^{18}\text{O}$ values between quartz and xenoliths (2.1–2.4‰) (Fig. 8), suggesting oxygen isotope near-equilibrium at tridymite crystallization temperature. Thus, the oxygen isotope data for quartz, tridymite, and whole-rock xenoliths indicate that these xenoliths retain their high-temperature (about 1100–1200 °C) oxygen isotope signatures, and that subsequent rapid cooling of the xenoliths mostly prevented resetting of oxygen isotopes at lower temperatures. The formation sequence of tridymite–hercynite xenoliths is summarized in Fig. 11.

4.4. Paleoclimate in southeast Asia

Paleosols can provide information about weathering and climatic conditions prevailing at the time of formation (Nesbitt and Young, 1982; Girard et al., 2000). Lateritic paleosols form by weathering in warm and humid tropical conditions that produce strongly desilicated clay minerals. The minimum formation age of the lateritic soils is the eruption age of the host basalts, which is about 15 Ma. The maximum formation age of the lateritic soils is the age of their source rocks. The nearby older basalts at Niutoushan, Tianmashan, Zhenhai, Liuhui, and Xiangshan, which are the best candidates for the source rocks of the lateritic soils, erupted as early as 17.1 ± 0.6 Ma (Ho et al., 2003). Thus, we conclude that strong leaching under tropical climate conditions existed in SE China during the interval from ~ 17 to 15 Ma.

A good measure of the degree of weathering can be obtained by calculation of the chemical index of alteration (CIA) using molecular proportions (Nesbitt and Young, 1982):

$$\text{CIA} = 100 \times \text{Al}_2\text{O}_3 / (\text{Al}_2\text{O}_3 + \text{CaO} + \text{Na}_2\text{O} + \text{K}_2\text{O}) \quad (2)$$

These xenoliths have CIA values between 96 and 99 (see Table 1), which are higher than those of Quaternary laterites (90–92) in SE China (Yang et al., 2000). Since the conditions to form Quaternary laterites

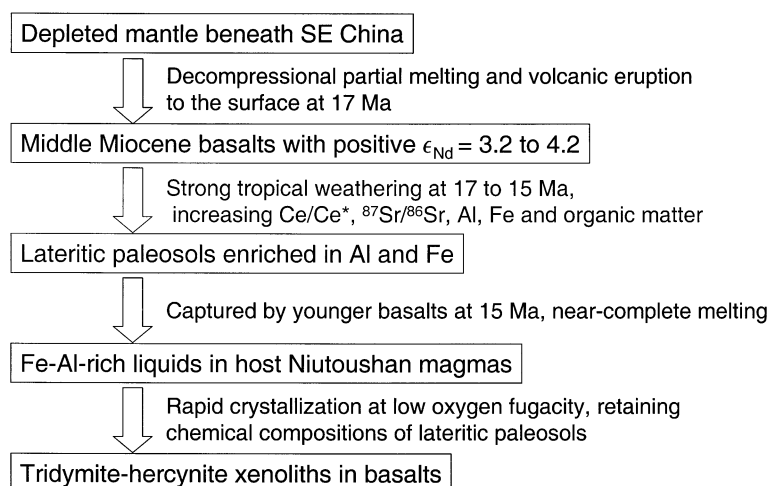


Fig. 11. Formation of the tridymite–hercynite xenoliths.

require annual average temperature of 19 °C and annual rainfall of 165 cm (Zhao and Yang, 1995), we infer that the conditions to form these Miocene (17–15 Ma) laterites would require annual average temperatures >19 °C and annual rainfall amounts >165 cm.

Interestingly, the time during which the lateritic paleosols were being produced (17–15 Ma) corresponds to a period of slow uplift of the Himalayan–Tibetan Plateau region, following the more rapid uplift and denudation of the Plateau at 21–17 Ma (Harrison et al., 1992; Hodges et al., 1992). The major uplift phase at 21–17 Ma coincides with a period of steepened slope of the $^{87}\text{Sr}/^{86}\text{Sr}$ ratio of seawater (Richter et al., 1992), and the associated increase in chemical weathering rates have postulated to have led to accelerated CO_2 consumption and thus climatic cooling (Raymo and Ruddiman, 1992). This phase of accelerated CO_2 consumption was followed by a period with reduced uplift rates and less chemical weathering as indicated by a flat seawater $^{87}\text{Sr}/^{86}\text{Sr}$ isotope curve at 16 Ma. The reduction in CO_2 consumption would have raised atmospheric CO_2 concentrations and climatic temperature. Additionally, eruptions of 17–15 Ma Columbia River flood basalts on the Colorado Plateau in northwest USA (Hodell and Woodruff, 1994), the Vogelsberg basalts from Central Europe (Schwarz, 1997), and the eastern China basalts could have contributed to a rising CO_2 concentration.

Evidence in support of a middle Miocene temperature maximum has come mainly from the oxygen isotopic record of deep ocean benthic foraminifer (Flower and Kennett, 1994), palaeobotanical data from Europe and North America (White et al., 1997), the distribution of ectothermic vertebrates of Central Europe (Bohme, 2003), and the occurrence of lateritic bauxite in central Germany (Schwarz, 1997). Our study provides additional evidence for a middle Miocene climatic optimum in East Asia from an unexpected source: hard rock xenoliths in basalts.

5. Summary

(1) The protoliths of tridymite–hercynite xenoliths are interpreted to have been lateritic paleosols that could have consisted mainly of halloysite, goethite, hematite, organic matter, and minor

amounts of CaCO_3 and BaSO_4 . There were few, if any, original quartz grains in the lateritic paleosols. The paleosols were captured and melted by hot basaltic lavas near the Earth's surface. The high viscosity (due to high total contents of $\text{SiO}_2 + \text{Al}_2\text{O}_3$) of the produced liquids and subsequent rapid cooling prevented the liquids from being assimilated/digested by host basaltic magmas, thus retaining the chemical and isotopic compositions (except for volatiles) of the paleosols.

- (2) The source rocks of the lateritic paleosols are probably nearby earlier basalts erupted as early as 17.1 Ma. Mesozoic granites, metasedimentary rocks, or volcanic rocks in the study region cannot be the source rocks for these lateritic paleosols.
- (3) The formation age of these paleosols is therefore between 17 and 15 Ma. This formation age corresponds to a period of slow uplift of the Himalayan–Tibetan Plateau region (and thus less consumption of CO_2) after 17 Ma, and the latest stage of the opening of the South China Sea (32–16 Ma), but preceded the collision of the Luzon arc with the Asian continent that started at 12 Ma BP.
- (4) The lateritic paleosols provide chemical evidence of intensive tropical weathering conditions in middle Miocene in SE China. The climatic conditions to form these middle Miocene laterites can be estimated as annual average temperatures >19 °C and annual rainfall of >165 cm. The slow uplift of the Himalayan–Tibetan plateau coupled with large global input of CO_2 from volcanic eruptions at 17–15 Ma may have contributed to the middle Miocene climatic optimum.
- (5) The contributions of Niutoushan and nearby earlier basalts to our understanding of middle Miocene climate are (1) to preserve the geochemical record of lateritic paleosols captured and transformed in the basalts; and (2) to provide robust constraints on the ages of the lateritic paleosols.

Acknowledgements

We are grateful to Suzanne Y. O'Reilly, Yuanming Pan, and Editor Roberta Rudnick for their

insightful reviews that significantly improved the quality of this paper. We are thankful to Xinmin Zhou for generously providing a field photo of the tridymite hercynite xenolith. We thank Yong-Fei Zheng, Vincent J.M. Salters, Roy Odom, Mary R. Reid, An Yin, Larry A. Taylor and Qu Qi for their help and fruitful discussions. This work was supported by NSF EAR-9805687 and NSF of China grant 40125007. We also acknowledge the support from the NSF Instrumentation and Facilities Program (EAR-0113563). [RR]

References

- Abouchami, W., Goldstein, S.L., Galer, S.J.G., Eisenhauer, A., Mangini, A., 1997. Secular changes of lead and neodymium in central Pacific seawater recorded by a Fe–Mn crust. *Geochim. Cosmochim. Acta* 61, 3957–3974.
- Anders, E., Grevesse, N., 1989. Abundances of the elements: meteoritic and solar. *Geochim. Cosmochim. Acta* 53, 197–214.
- Banfield, J.F., Eggleton, R.A., 1989. Apatite replacement and rare earth mobilization, fractionation, and fixation during weathering. *Clays Clay Miner.* 37, 113–127.
- Basu, A.R., Wang, J.W., Huang, W.K., Xie, G.H., Tatsumoto, M., 1991. Major element, REE, and Pb, Nd and Sr isotopic geochemistry of Cenozoic volcanic rocks of eastern China: implications for their origin from suboceanic-type mantle reservoirs. *Earth Planet. Sci. Lett.* 105, 149–169.
- Ben Othman, D., White, W.M., Patchett, J., 1989. The geochemistry of marine sediments, island arc magma genesis, and crust–mantle recycling. *Earth Planet. Sci. Lett.* 94, 1–21.
- Bohme, M., 2003. The Miocene Optimum: evidence from ectothermic vertebrates of Central Europe. *Palaeogeogr. Palaeoclimatol. Palaeoecol.* 195, 389–401.
- Braun, J.J., Pagel, M., Muller, J.P., Bilong, P., Michard, A., Guillet, B., 1990. Cerium anomalies in lateritic profiles. *Geochim. Cosmochim. Acta* 54, 781–795.
- Chen, D.G., Zhang, J.B., 1992. Nd, Sr, Pb isotopes and K–Ar age of basaltic rocks in Longhai and Mingxi, Fujian province. *Acta Petrol. Sin.* 8, 324–331.
- Chung, S.L., Sun, S.S., Tu, K., Chen, C.H., Lee, C.Y., 1994. Late Cenozoic basaltic volcanism around the Taiwan Strait, SE China: product of lithosphere–asthenosphere interaction during continental extension. *Chem. Geol.* 112, 1–20.
- Chung, S.L., Jahn, B.M., Chen, S.J., Lee, T., Chen, C.H., 1995. Miocene basalts in northwestern Taiwan: evidence for EM-type mantle sources in the continental lithosphere. *Geochim. Cosmochim. Acta* 59, 549–555.
- Deer, W.A., Howie, R.A., Zussman, J., 1992. *An Introduction to Rock-Forming Minerals*. Longman, New York. 696 pp.
- Dixon, S., Rutherford, M.J., 1979. Plagiogranites and late-stage immiscible liquids in ophiolites and mid-ocean ridge suites: an experimental study. *Earth Planet. Sci. Lett.* 45, 45–60.
- Fan, W.M., Zhang, H.F., Baker, J., Jarvis, K.E., Mason, P.R.D., Menzies, M.A., 2000. On and off the North China craton: where is the Archean keel? *J. Petrol.* 41, 933–950.
- Flower, B.P., Kennett, J.P., 1994. The middle Miocene climatic transition: East Antarctic ice sheet development, deep ocean circulation and global carbon cycling. *Palaeogeogr. Palaeoclimatol. Palaeoecol.* 108, 537–555.
- German, C.R., Elderfield, H., 1990. Application of the Ce anomaly as a paleoredox indicator: the ground rules. *Paleoceanography* 5, 823–833.
- Girard, J.P., Freyssinet, P., Chazot, G., 2000. Unraveling climatic changes from intraprofile variation in oxygen and hydrogen isotopic composition of goethite and kaolinite in laterites: an integrated study from Yaou, French Guiana. *Geochim. Cosmochim. Acta* 64, 409–426.
- Harrison, T.M., Copeland, P., Kidd, W.S.F., Yin, A., 1992. Raising Tibet. *Science* 255, 1663–1670.
- Ho, K.S., Chen, J.C., Smith, A.D., Juang, W.S., 2000. Petrogenesis of two groups of pyroxenite from Tungchihsu, Penghu Islands, Taiwan Strait: implications for mantle metasomatism beneath SE China. *Chem. Geol.* 167, 355–372.
- Ho, K.S., Chen, J.C., Lo, C.H., Zhao, H.L., 2003. ⁴⁰Ar–³⁹Ar dating and geochemical characteristics of late Cenozoic basaltic rocks from the Zhejiang–Fujian region, SE China: eruption ages, magma evolution and petrogenesis. *Chem. Geol.* 197, 287–318.
- Hodell, D.A., Woodruff, F., 1994. Variations in the strontium isotopic ratio of seawater during the Miocene: stratigraphic and geochemical implications. *Paleoceanography* 9, 405–426.
- Hodges, K.V., Parrish, R., Housch, T., Lux, D., Chen, Z., 1992. Simultaneous Miocene extension and shortening in the Himalayan Orogen. *Science* 258, 1466–1470.
- Hofmann, A.W., 1988. Chemical differentiation of the Earth: the relationship between mantle, continental crust, and the oceanic crust. *Earth Planet. Sci. Lett.* 90, 297–314.
- Huang, X., Sun, S.H., DePaolo, D.J., Wu, K.L., 1986. Nd–Sr isotope study of Cretaceous magmatic rocks from Fujian province. *Acta Petrol. Sin.* 2, 50–63.
- Lin, Y.K., 1992. Cenozoic basalts and their volcanism in Tianma–Niutou shan area, Fujian province. *Acta Petrol. Sin.*, (4), 376–385.
- McLennan, S.M., 1989. Rare earth elements in sedimentary rocks: influence of provenance and sedimentary processes. *Rev. Mineral.* 21, 169–200.
- Morey, G.B., Setterholm, D.R., 1997. Rare earth elements in weathering profiles and sediments of Minnesota: implications for province studies. *J. Sediment. Res.* 67, 105–115.
- Nesbitt, H.W., Young, G.M., 1982. Early Proterozoic climates and plate motions inferred from major element chemistry of lutes. *Nature* 299, 715–717.
- Nguyen, H., Flower, M.F.J., Carlson, R.W., 1996. Major, trace element, and isotopic compositions of Vietnamese basalts: interaction of hydrous EM1-rich asthenosphere with thinned Eurasian lithosphere. *Geochim. Cosmochim. Acta* 60, 4329–4351.
- Pan, Y., Stauffer, M.R., 2000. Cerium anomaly and Th/U fraction-

- ation in the 1.85 Ga Flin Flon Paleosol: clues from REE- and U-rich accessory minerals and implications for paleoatmospheric reconstruction. *Am. Mineral.* 85, 898–911.
- Piper, D.Z., 1974. Rare earth elements in ferromanganese and other marine phases. *Geochim. Cosmochim. Acta* 29, 1007–1022.
- Price, R.C., Gray, C.M., Wilson, R.E., Frey, F.A., Taylor, S.R., 1991. The effects of weathering on rare-earth element, Y and Ba abundances in Tertiary basalts from southeastern Australia. *Chem. Geol.* 93, 245–265.
- Qi, Q., Taylor, L.A., Zhou, X.M., 1994. Petrology and geochemistry of an unusual tridymite–hercynite xenolith in tholeiite from southeastern China. *Mineral. Petrol.* 50, 195–207.
- Qi, Q., Taylor, L.A., Zhou, X.M., 1995. Petrology and geochemistry of mantle peridotite xenoliths from SE China. *J. Petrol.* 36, 55–79.
- Raymo, M.E., Ruddiman, W.F., 1992. Tectonic forcing of late Cenozoic climate. *Nature* 359, 117–122.
- Rhodes, J.M., 1996. Geochemical stratigraphy of lava flows sampled by the Hawaii Scientific drilling project. *J. Geophys. Res.* 101, 11729–11746.
- Richter, F.M., Rowley, D.B., DePaolo, D.J., 1992. Sr isotope evolution of seawater: the role of tectonics. *Earth Planet. Sci. Lett.* 109, 11–23.
- Schairer, J.F., Yagi, K., 1952. The system FeO–Al₂O₃–SiO₂. *Am. J. Sci.*, (Part 2), 471–512 (Bowen Volume).
- Schwarz, T., 1997. Lateritic bauxite in central Germany and implications for Miocene palaeoclimate. *Palaeogeogr. Palaeoclimatol. Palaeoecol.* 129, 37–50.
- Song, Y., Frey, F.A., 1989. Geochemistry of peridotite xenoliths in basalt from Hannuoba, Eastern China: implications for subcontinental mantle heterogeneity. *Geochim. Cosmochim. Acta* 53, 97–113.
- Stracke, A., Zindler, A., Salters, V.J.M., McKenzie, D., Blichert-Toft, J., Albarede, F., Gronvold, K., 2003. Theistareykir revisited. *Geochem. Geophys. Geosyst.* 4, 8507 (doi:10.1029/2001GC000201).
- Sun, S.S., McDonough, W.F., 1989. Chemical and isotopic systematics of oceanic basalts: implications for mantle composition and processes. In: Saunders, A.D., Norry, M.J. (Eds.), *Magma-tism in the Ocean Basins*. Geological Society Special Publication, Oxford, pp. 313–345.
- Takahashi, H., Takeuchi, N., Ishida, S., Wakamatsu, M., 2000. Oxygen evolution and chemical state changes of iron during firing of red clay bodies at low oxygen pressure. *J. Ceram. Soc. Jpn.* 108, 705–709.
- Tapponnier, P., Peltzer, G., Armijo, R., 1986. On the mechanics of the collision between India and Asia collision tectonics. In: Ramsey, J.G., Coward, M.P., Ries, A.C. (Eds.), *Collision Tectonics*. Geol. Soc. Spec. Pub., London, pp. 115–157.
- Tatsumi, Y., Otofujii, Y., Matsuda, T., Nohda, S., 1989. Opening of the Sea of Japan back-arc basin as asthenospheric injection. *Tectonophysics* 166, 317–329.
- Tatsumoto, M., Basu, A.R., Huang, W., Wang, J.W., Xie, G.H., 1992. Sr, Nd, and Pb isotopes of ultramafic xenoliths in volcanic rocks of Eastern China: enriched components EM1 and EM2 in subcontinental lithosphere. *Earth Planet. Sci. Lett.* 113, 107–128.
- Tlig, S., Steinberg, M., 1982. Distribution of rare-earth elements (REE) in size fractions of recent sediments of the Indian Ocean. *Chem. Geol.* 37, 317–333.
- Todt, W., Cliff, R.A., Hanser, A., Hofmann, A.W., 1996. Evaluation of a ²⁰²Pb–²⁰⁵Pb double spike for high-precision lead isotope analysis. In: Basu, A.R., Hart, S.R. (Eds.), *Earth Processes: Reading the Isotopic Code*. Geophysical Monograph Am. Geophys. Union, Washington, DC, pp. 429–437.
- Tu, K., Flower, M.F.J., Carlson, R.W., Zhang, M., Xie, G.H., 1991. Sr, Nd, and Pb isotopic compositions of Hainan basalts (south China): Implications for a subcontinental lithosphere Dupal source. *Geology* 19, 567–569.
- White, J.M., Ager, T.A., Adam, D.P., Leopold, E.B., Liu, G., Jette, H., Schweger, C.E., 1997. An 18 million year record of vegetation and climate change in northwestern Canada and Alaska: tectonic and global climatic correlates. *Palaeogeogr. Palaeoclimatol. Palaeoecol.* 130, 293–306.
- Xie, X.J., Yan, M., Wang, C., Li, L., Shen, H., 1989. Geochemical reference samples: GSD9-12, GSS1-8, GSR1-6. *Geostand. Newsl.* 13, 83–179.
- Xie, X., Xu, X.S., Zou, H.B., Xing, G.F., 2001. Trace element and Nd–Sr–Pb isotope studies of Mesozoic and Cenozoic basalts in coastal area of SE China. *Acta Petrol. Sin.* 17, 617–628.
- Xu, X.S., O'Reilly, S.Y., Griffin, W.L., Zhou, X.M., 2003. Enrichment of upper mantle peridotite: petrological, trace element and isotopic evidence in xenoliths from SE China. *Chem. Geol.* 198, 163–188.
- Yang, Y.G., Liu, C.Q., Yuan, K.N., He, Z.L., 2000. Laterite formation process in southern China and its rare earth element geochemistry. *Quat. Sci.* 20, 469–480.
- Yu, X.Y., 1985. The origin of basaltic rocks in Nioutoushan area—high pressure differentiation. *Chin. J. Geochem.* 4, 150–158.
- Zhao, Q.G., Yang, H., 1995. A preliminary study of red earth and changes of Quaternary environment in south China. *Quat. Sci.* 15, 107–116.
- Zhao, Z.F., Zheng, Y.F., 2003. Calculation of oxygen isotope fractionation in magmatic rocks. *Chem. Geol.* 193, 59–80.
- Zheng, Y.F., 1991. Calculation of oxygen isotope fractionation in metal oxides. *Geochim. Cosmochim. Acta* 55, 2299–2307.
- Zheng, Y.F., 1993. Calculation of oxygen isotope fractionation in anhydrous silicate minerals. *Geochim. Cosmochim. Acta* 57, 1079–1091.
- Zheng, Y.F., 1995. Oxygen isotope fractionation in magnetites: structural effect and oxygen inheritance. *Chem. Geol.* 121, 309–316.
- Zheng, Y.F., 1999. On calculation of oxygen isotope fractionation in minerals. *Episodes* 22, 99–106.
- Zhou, X.M., 1981. An investigation of two basaltic series and their inclusions in Nioutoushan of Fujian Province of southeastern China. *Bull. Nanjing Univ.* 3, 382–392.
- Zhou, X.M., 1983. Discovery of tridymite–hercynite xenoliths in basalts. *Chin. Sci. Bull.* 28, 486–489.
- Zhou, X.H., Armstrong, R.L., 1982. Cenozoic volcanic rocks of eastern China—secular trends in chemistry and strontium isotopic composition. *Earth Planet. Sci. Lett.* 58, 301–329.

- Zindler, A., Hart, S.R., 1986. Chemical geodynamics. *Annu. Rev. Earth Planet. Sci.* 14, 493–571.
- Zou, H., Zindler, A., Xu, X.S., Qi, Q., 2000. Major and trace element, and Nd–Sr–Pb isotope studies of Cenozoic basalts in SE China: mantle sources, regional variations, and tectonic significance. *Chem. Geol.* 171, 33–47.
- Zou, H., Reid, M.R., Liu, Y.S., Yao, Y.P., Xu, X.S., Fan, Q.C., 2003. Constraints on the origin of historic potassic basalts from northeast China by U–Th disequilibrium data. *Chem. Geol.* 200, 189–201.